Real-Time Detection of the Dynamic Eccentricity in Permanent-Magnet Synchronous Motors by Monitoring Speed and Back EMF Induced in an Additional Winding

Kyungjin Kang, Jeongyong Song, Chiho Kang, Sangjin Sung, and Gunhee Jang, *Member, IEEE*

***Abstract*—We developed a real-time method to detect the dynamic eccentricity of a rotor in a permanent-magnet (PM) motor by monitoring a fault detection signal induced in an additional winding, without performing any further postprocessing, even under a nonstationary rotational speed. After deriving a mathematical equation of the back electromotive force (EMF) induced in a tooth-coil winding, we proposed a fault detection signal, which is the back EMF in an additional winding divided by the rotational speed, when the additional winding is wound around the teeth corresponding to an even number of pole pitches. We used the 2-D finite-element model of a three-phase PM motor with eight poles and 12 slots to verify the proposed method. We also developed an experimental setup which can change the dynamic eccentricity of a PM motor and we performed the experiment for PM motors with dynamic eccentricities of 0%, 25%, and 50% to verify the proposed method. Through the mathematical equation, numerical simulation, and experiment, we confirmed that the fault detection signal proposed in this paper can successfully detect the dynamic eccentricity in a PM motor in real time.**

***Index Terms*—Dynamic eccentricity, fault diagnosis, permanent-magnet (PM) motors.**

I. Introduction

ELECTRIC motors are popular power generation devices for various applications in vehicles, home appliances, and industrial equipment. A motor fault decreases the motor lifespan and adversely affects the sound operation of the motor or the entire motor-driven system, and it may cause a shutdown. The ability to detect a motor fault in advance has been an important topic in maintaining the reliability of motors and motor-driven systems, because it would allow engineers to fix the fault or to replace the motor in advance before it shuts down the entire system or causes serious damage. Bonnett and Yung [1] provided the statistical information that 69% of faults of the induction motors with the output power ranging from 1 to 200 hp originate from the breakdown of bearings. Bearing faults, which are major motor faults, are caused by insufficient lubrication, irregular contact, heavy radial, and axial stress due to unbalanced rotor inertia, magnetic pull of the rotor, poor mounting, or misalignment [2]. Bearing faults lead to abnormal vibration and acoustic noise due to increased wear and uneven contact. Many studies have investigated ball bearing faults, which can be identified by detecting the defect frequencies of the ball bearings in vibrations and acoustic noise [3]–[7]. The defect frequencies of ball bearings are generated due to cracks or irregular curvatures of the balls, inner and outer races, or abnormal contact between balls and races. However, defect frequencies exist only in motors using ball bearings and only after the ball bearing faults are well progressed. Some signals are generated by the motors before motor failure, including signals of a rotor's static or dynamic eccentricities. As shown in Fig. 1, the motion of a rotor can be classified into concentric, static, and dynamic eccentric motions. In an ideal case of concentric motion, the rotor concentrically rotates with respect to the center of stator and it has uniform air gap because the center of rotor coincides the center of stator. In static eccentric motion, the rotor rotates around the center of rotor and the air gap is not uniform but it never changes (the position of the minimum air gap is fixed in the space). Mirimani *et al.* [8] proposed a method to detect the static eccentricity in single-stator–single-rotor axial-flux permanent-magnet (PM) machines by comparing the amplitudes of back electromotive forces (EMFs) induced in the four coils of one phase, but in dynamic eccentric motion, the rotor rotates around the center of rotor with a whirling motion, so the position of the minimum air gap revolves around the center of the stator, which changes the magnetic field concurrently. The uneven magnetic field in the air gap generates unbalanced magnetic forces. Dynamic eccentricity also increases rotating unbalance of a rotor with respect to the center of revolution and it generates centrifugal force concurrently. Unbalanced magnetic force and centrifugal force excite the bearing periodically and the dynamic eccentric motion may grow when they exceed the load capacity of bearing.

Manuscript received November 21, 2016; revised February 8, 2017; accepted March 10, 2017. Date of publication March 22, 2017; date of current version August 9, 2017. This work was supported by the National Research Foundation of Korea grant funded by the Korean Government (MSIP) (2015R1A2A1A05001837). *(Corresponding author: Gunhee Jang.)*

The authors are with the Department of Mechanical Convergence Engineering, Hanyang University, Seoul 04763, South Korea (e-mail: jin795@hanyang.ac.kr; othrys@hanyang.ac.kr; cho666k@naver.com; s_symbol@hanmail.net; ghjang@hanyang.ac.kr).

Color versions of one or more of the figures in this paper are available online at http://ieeexplore.ieee.org.

Digital Object Identifier 10.1109/TIE.2017.2686376

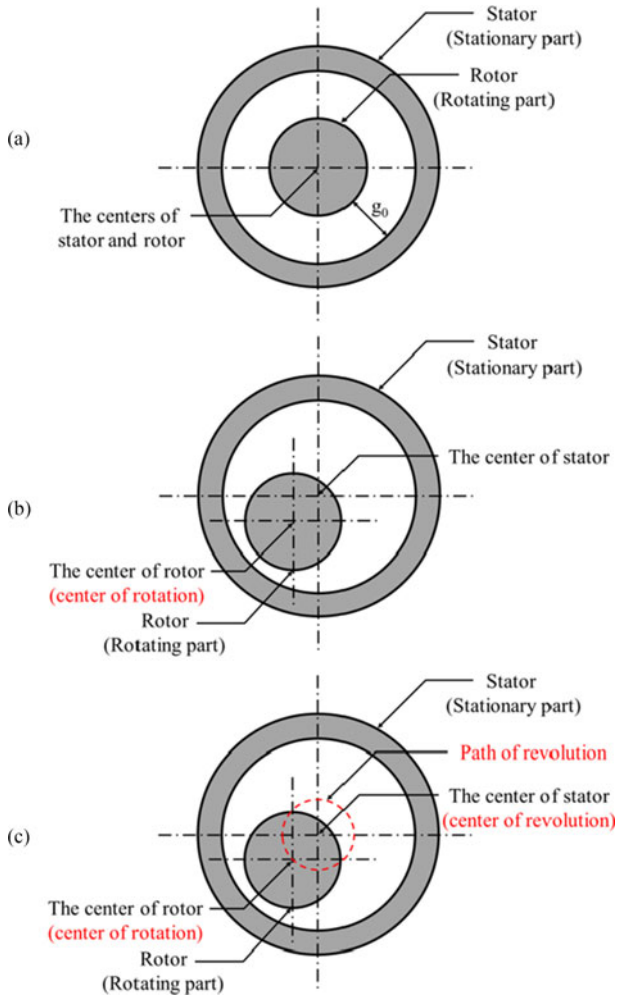

Fig. 1. Motion of a rotor (a) without eccentricity, (b) with static eccentricity, and (c) with dynamic eccentricity.

It may eventually cause bearing faults because the bearing is the most flexible and vulnerable component of the motor. Monitoring the dynamic eccentricity of a rotor may be an effective method to predict motor faults.

Many researchers have studied various methods to detect dynamic eccentricity of PM motors and generators by monitoring the supply current [9]–[17], inductance [18], [19], torque [20], vibration [21], and noise [22], [23]. They utilized various signal processing techniques, such as fast Fourier transform [9], [12], [17], wavelet transform [10], [11], power spectral density [13]–[15], [21], and fuzzy logic [16]. Rosero *et al.* [10], [11] studied a monitoring technique to detect the dynamic eccentricity of PM motors by applying a continuous wavelet transformation method to the supply current. However, their method can only be applied to detect dynamic eccentricity of a PM motor with a stationary rotational speed. Rajagopalan *et al.* [12] also suggested a method to detect dynamic eccentricity of PM motors by monitoring the variation of the supply current due to the change of commutation angle. Their method was restricted to PM motors using hall sensors to detect rotor positions for commutation, and they utilized the change of hall sensor signals due to dynamic eccentricity to identify the change of the commutation angle. Ebrahimi *et al.* [13]–[16] proposed a method to detect the dynamic eccentricity of PM motors by identifying the sideband frequencies in the power spectral density of the driving current. However, it is very difficult for their methods to be applied in real applications to detect dynamic eccentricity because the amplitudes of the sideband frequencies of the supply current are too small (−80 dB with respect to the main harmonic component of the supply current). Also, these methods can only be utilized to detect dynamic eccentricity of a PM motor with a stationary rotational speed. Bruzzese [17] suggested a method to detect dynamic eccentricity in synchronous machines by monitoring the unbalance caused in the split-phase currents. However, this method requires a postprocessing technique of the acquired signal, which makes it difficult to be applied in real time to detect the dynamic eccentricity of a rotor. This method also cannot be utilized to detect the dynamic eccentricity of a synchronous machine with a nonstationary rotational speed. Hong *et al.* [18], [19] proposed a method to detect the dynamic eccentricity of PM motors by monitoring the *d*-axis inductance. However, their research cannot be utilized in surface-mounted PM motors because only interior PM motors have an inductance difference between the *d* and *q*-axes. Rezig *et al.* [22], [23] suggested a method to detect dynamic eccentricity of PM motors by monitoring an acoustic noise. However, it is difficult to identify the dynamic eccentricity of the PM motor with a fan or disk, because the acoustic noise due to eccentricity and the aero acoustic noise due to the fan or disk are blended. The conventional methods need not only sensors to measure supply current, inductance, torque, vibration, and noise but also additional postprocessing, such as frequency analysis. They may not effectively detect the dynamic eccentricity under nonstationary rotational speed.

In this paper, we proposed a method to detect the dynamic eccentricity of a rotor in a PM motor by monitoring a fault detection signal induced in an additional winding in real time, without performing further postprocessing, even under nonstationary rotational speeds. This paper is organized as follows. In Section II, we derived a mathematical equation for the back EMF induced in a tooth-coil winding due to the dynamic eccentricity of surface-mounted PM motors. We proposed a fault detection signal, which is the back EMF in an additional winding divided by the rotational speed, when the additional winding is wound around the teeth corresponding to an even number of pole pitches. In Section III, we developed a finite-element model to verify the proposed method. In Section IV, we performed the experiment for PM motors with dynamic eccentricities of 0%, 25%, and 50%, by using concentric and eccentric shaft housings. Finally, Section V gives the conclusions.

II. Mathematical Formulation of Back EMF Due to Dynamic Eccentricity

A. Back EMF Induced in a Tooth-Coil Winding Without Eccentricity

When a rotor exhibits concentric motion without eccentricity, the air-gap length of the motor is constant, regardless of the

position of the rotor, as shown in Fig. 1(a)

$$g_{\mathrm{ideal}} = g_0 \tag{1}$$

where g_0 is the inherent air-gap length of a motor without eccentricity. The relative permeance of the air gap without eccentricity can be represented as follows [24], [25]:

$$\Lambda_{\mathrm{ideal}} = \frac{\mu_0 \mu_{\mathrm{PM}}}{k_c g_0 \mu_{\mathrm{PM}} + h_{\mathrm{PM}}} \tag{2}$$

where μ_0, k_c, h_{PM}, and μ_{PM} are the permeability of free space, Carter's gap coefficient, the radial thickness of the PM, and the relative permeability of the PM, respectively. The magnetomotive force (MMF) F originating from the PM can be represented by using the Fourier series as follows:

$$F = F_{\mathrm{PM}} \cdot \sum_{k=1}^{\infty} \cos\left(kp\theta - kp\omega t - \phi\right) \tag{3}$$

where F_{PM}, p, θ, ω, t, and ϕ are the magnitude of the MMF, the number of pole pairs, angle from the x-axis, angular velocity, time, and the phase of the MMF, respectively. The magnetic flux density of the air gap B can be calculated as the product of the MMF and the relative permeance of the air gap, as follows [17], [24]–[26]:

$$B = F \cdot \Lambda. \tag{4}$$

The magnetic flux passing through a tooth Φ can be calculated by integrating the magnetic flux density along the air gap facing a tooth as follows:

$$\Phi_l = \int B \cdot dA = H_{\mathrm{PM}} \int_{\frac{2\pi}{s}(l-1)}^{\frac{2\pi}{s}l} B \cdot r d\theta \tag{5}$$

where H_{PM}, s, l, and r are the height of the PM in the axial direction, the total number of slots, the lth tooth, and the radius of the air gap from the center of the stator, respectively. The back EMF induced in the lth tooth-coil winding E_l can be calculated as the derivative of the magnetic flux passing through the lth tooth with respect to time as follows:

$$E_l = -N\frac{d\Phi}{dt} \tag{6}$$

where N is the number of turns. After substituting (2) and (3) into (4), integrating along the air gap facing a tooth, and then differentiating with respect to time, the back EMF induced in the lth tooth-coil winding of the PM motor, without eccentricity, can be represented as follows.

$$E_{\mathrm{ideal}\_l} = -\frac{2NF_{\mathrm{PM}}H_{\mathrm{PM}}\mu_0\mu_{\mathrm{PM}}r\omega}{k_c g_0 \mu_{\mathrm{PM}} + h_{\mathrm{PM}}} \cdot \sum_{k=1}^{\infty}\left\{\sin\left(kp\frac{\pi}{s}\right)\sin\left(kp\frac{\pi}{s}(2l-1) - kp\omega t - \phi\right)\right\}. \tag{7}$$

For a PM motor without dynamic eccentricity, the back EMF induced in a tooth-coil winding changes sinusoidally with the pth multiple harmonics under a stationary rotational speed.

B. Back EMF Induced in a Tooth-Coil Winding With Dynamic Eccentricity of a Rotor

Fig. 1(c) shows the motion of a rotor with dynamic eccentricity, in which the centers of the rotor and the stator are different. The rotor both rotates around its own center and revolves around the center of the stator. The air gap can be represented as a function of space and time as follows [24]–[26]:

$$g_{\mathrm{dyn}} = g_0\left\{1 - \frac{\varepsilon}{g_0}\cos\left(\theta - \omega t - \varphi\right)\right\} \tag{8}$$

where ε and φ are the magnitude of the eccentricity and initial position of the minimum air gap, respectively. The relative permeance of the air gap with dynamic eccentricity can be represented as follows [24], [25]:

$$\Lambda_{\mathrm{dyn}} = \frac{\mu_0}{k_c g_0\left\{1 - \frac{\varepsilon}{g_0}\cos\left(\theta - \omega t - \varphi\right)\right\} + \frac{h_{\mathrm{PM}}}{\mu_{\mathrm{PM}}}}. \tag{9}$$

After applying a Taylor series and neglecting higher order terms, the relative permeance of the air gap with dynamic eccentricity can be represented as follows [24], [25]:

$$\Lambda_{\mathrm{dyn}} = \frac{\mu_0\mu_{\mathrm{PM}}}{k_c g_0 \mu_{\mathrm{PM}} + h_{\mathrm{PM}}} + \frac{\mu_0 {\mu_{\mathrm{PM}}}^2 \varepsilon k_c}{\left(k_c g_0 \mu_{\mathrm{PM}} + h_{\mathrm{PM}}\right)^2}\cos\left(\theta - \omega t - \varphi\right). \tag{10}$$

After substituting (10) and (3) into (4), integrating along the air gap facing a tooth, and then differentiating with respect to time, the back EMF induced in the lth tooth-coil winding of the PM motor with dynamic eccentricity can be represented as follows:

$$E_{\mathrm{dyn}\_l} = -\frac{2NF_{\mathrm{PM}}H_{\mathrm{PM}}\mu_0\mu_{\mathrm{PM}}r\omega}{k_c g_0 \mu_{\mathrm{PM}} + h_{\mathrm{PM}}} \cdot \sum_{k=1}^{\infty}\left\{\sin\left(kp\frac{\pi}{s}\right)\sin\left(kp\frac{\pi}{s}(2l-1) - kp\omega t - \phi\right)\right\} - \frac{NF_{\mathrm{PM}}H_{\mathrm{PM}}\mu_0{\mu_{\mathrm{PM}}}^2\varepsilon k_c r\omega}{\left(k_c g_0 \mu_{\mathrm{PM}} + h_{\mathrm{PM}}\right)^2} \cdot \sum_{k=1}^{\infty}\left\{\sin\left((kp \pm 1)\frac{\pi}{s}\right) \sin\begin{pmatrix}(kp \pm 1)\frac{\pi}{s}(2l-1) \\ -(kp \pm 1)\omega t - \phi \mp \varphi\end{pmatrix}\right\}. \tag{11}$$

The back EMF induced in the lth tooth-coil winding has additional $(kp \pm 1)$ components due to the dynamic eccentricity under a stationary rotational speed. The additional components of the back EMF are linearly proportional to the amplitude of eccentricity.

C. Back EMF Induced in a Phase Winding

For a PM motor with series connections between tooth-coil windings, the back EMF induced in a phase winding can be calculated as a sum of the back EMF induced in the teeth-coil

windings of the same phase, as follows:

$$\begin{aligned} E_{\text{ideal\_phase\_}U} &= E_{\text{dyn\_phase\_}U} \\ &= \frac{2NF_{\text{PM}}H_{\text{PM}}\mu_0\mu_{\text{PM}}r\omega s}{P_{\text{phase}}\left(k_c g_0 \mu_{\text{PM}} + h_{\text{PM}}\right)} \\ &\quad \cdot \sum_{k=1}^{\infty} \left\{ \begin{array}{l} \sin\left(kp\frac{\pi}{s}\right) \\ \sin\left(kp\frac{\pi}{s} - kp\omega t - \phi\right) \end{array} \right\} \end{aligned} \tag{12}$$

where P_{phase} is the number of phases. On the other hand, for a PM motor using concentric winding with parallel connections between tooth-coil windings, the back EMF induced in a phase winding can be calculated as an average of the back EMFs induced in the teeth-coil windings of the same phase. The additional components of the back EMF induced in a phase winding originating from the dynamic eccentricity cancel each other out during the summation or averaging process due to the differences of phases regardless of the winding pattern. The back EMFs induced in the phase winding of the PM motor without and with dynamic eccentricity are the same. Therefore, the mathematical equations show that changes of dynamic eccentricities cannot be identified by monitoring the back EMF induced in a phase winding.

D. Back EMF Induced in a Tooth-Coil Winding Under Nonstationary Rotational Speed

Under the nonstationary rotational speed of $\omega_0 + d\omega$, the back EMF induced in the lth tooth-coil winding of the PM motor without eccentricity can be represented by substituting $\omega_0 + d\omega$ into (7) as follows:

$$\begin{aligned} E_{\text{ideal\_}l} = &- \frac{2NF_{\text{PM}}H_{\text{PM}}\mu_0\mu_{\text{PM}}r\left(\omega_0 + d\omega\right)}{k_c g_0 \mu_{\text{PM}} + h_{\text{PM}}} \\ &\cdot \sum_{k=1}^{\infty} \left\{ \sin\left(kp\frac{\pi}{s}\right) \sin\left(kp\frac{\pi}{s}(2l-1)\right. \right. \\ &\left. \left. - kp\left(\omega_0 + d\omega\right)t - \phi\right) \right\} \end{aligned} \tag{13}$$

where ω_0 and $d\omega$ are the stationary rotational speed and the instantaneous increase of rotational speed, respectively. The amplitude of the back EMF induced in a tooth-coil winding is linearly proportional to the instantaneous rotational speed. The frequency of the back EMF induced in a tooth-coil winding is $kp(\omega_0 + d\omega)/\omega_0$ with respect to the stationary rotational frequency, and the frequency increases by the amount $kpd\omega/\omega_0$ under a nonstationary rotational speed. In the case of $kpd\omega/\omega_0 = \pm 1$, the frequency of the back EMF induced in a tooth-coil winding is $(kp \pm 1)$, which is the same as the frequency component due to the dynamic eccentricity under stationary rotational speed as shown in (11). Therefore, monitoring the additional $(kp \pm 1)$ components of back EMF induced in a tooth-coil winding cannot be sufficient to identify the dynamic eccentricity of a PM motor under a nonstationary rotational speed.

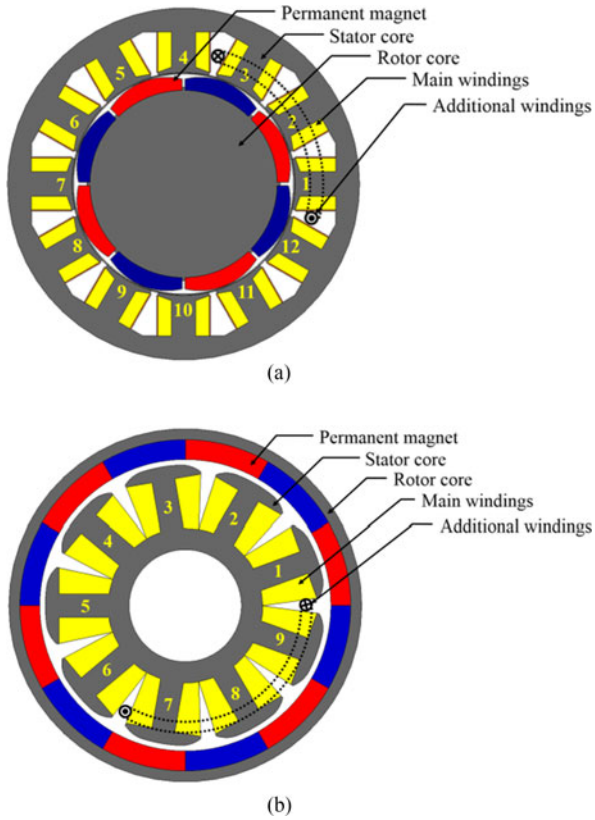

Fig. 2. Additional winding for (a) three-phase PM motor with eight poles and 12 slots and (b) three-phase PM motor with 12 poles and nine slots.

E. Proposed Method to Detect the Dynamic Eccentricity

We propose a method to detect the dynamic eccentricity of a rotor in a PM motor by monitoring the back EMF induced in an additional winding wound around the teeth corresponding to an even number of pole pitches. Fig. 2 shows how to wind the additional winding. In the case of a PM motor with eight poles and 12 slots, the additional winding can be wound around three consecutive teeth because three teeth face two poles, as shown in Fig. 2(a). In the case of a PM motor with 12 poles and nine slots, the additional winding can be wound around three consecutive teeth because three teeth face four poles, as shown in Fig. 2(b). The back EMF induced in an additional winding can be calculated as a sum of the back EMFs induced in the tooth-coil wound around the teeth corresponding to an even number of pole pitches. The amplitude of the back EMF is linearly proportional to the rotational speed. Therefore, we propose a fault detection signal to detect the dynamic eccentricity as the back EMF induced in the additional winding divided by rotational speed as follows:

$$S_{\text{fault}} = \sum_{l=1}^{m} \frac{E_l}{\omega} \tag{14}$$

where m is the number of teeth corresponding to the even number of pole pitches. The back EMF in (14) can be determined by measuring the voltage of the additional winding and the rotational speed can be determined by the zero crossing of the

back EMF induced in phase windings. In this way, the proposed method can also be applied to the case of a nonstationary rotational speed. The fault detection signal induced in the additional winding of the PM motor without eccentricity can be calculated to be zero, due to the phase differences between the back EMFs induced in tooth-coil windings corresponding to the even number of pole pitches

$$S_{\text{fault\_ideal}} = \sum_{l=1}^{m} \frac{E_{\text{ideal\_}l}}{\omega} = 0. \tag{15}$$

The fault detection signal induced in an additional winding of the PM motor with dynamic eccentricity can be calculated as follows:

$$\begin{aligned} S_{\text{fault\_dyn}} &= \sum_{l=1}^{m} \frac{E_{\text{dyn\_}l}}{\omega} \\ &= -\frac{N F_{\text{PM}} H_{\text{PM}} \mu_0 {\mu_{\text{PM}}}^2 \varepsilon k_c r}{\left(k_c g_0 \mu_{\text{PM}} + h_{\text{PM}}\right)^2} \\ &\quad \cdot \sum_{l=1}^{m} \sum_{k=1}^{\infty} \left\{ \sin\left((kp \pm 1)\frac{\pi}{s}\right) \right. \\ &\quad \left. \sin\left(\begin{matrix}(kp \pm 1)\frac{\pi}{s}(2l-1) \\ -(kp \pm 1)\omega t - \phi \mp \varphi\end{matrix}\right) \right\}. \end{aligned} \tag{16}$$

The fault detection signal induced in the additional winding is generated as shown in (16) due to the dynamic eccentricity in a PM motor because the additional components of the back EMF induced in each tooth-coil winding in (11) do not cancel out during the summation process. The magnitude of the fault detection signal can be utilized to monitor the dynamic eccentricity of a rotor in a PM motor in real time without further performing fast Fourier transformations of the fault detection signal, because it is generated only when the dynamic eccentricity exists. The proposed method can also detect the dynamic eccentricity of a PM motor even under nonstationary rotational speeds because the fault detection signal is not dependent on speed. The proposed method can be utilized only in motors with a rotationally symmetric structure, which rotationally repeat the patterns of two poles and three slots, or four poles and three slots, because the additional winding, wound around three consecutive slots corresponding to an even number of pole pitches, generates the fault detection signal for dynamic eccentricity.

III. Finite-Element Analysis

The proposed mathematical equations make it possible to predict the fault detection signal induced in a tooth-coil winding, a phase winding, and an additional winding generated by the dynamic eccentricity. However, they cannot predict the magnitudes of the back EMF due to the complex geometry of the PM motors and the nonlinear characteristics of the magnetic materials. We utilized a finite-element analysis to verify the proposed mathematical equations, as well as to determine the amplitudes of the fault detection signal induced in an additional winding generated by dynamic eccentricity.

TABLE I
Major Specifications of the PM Motor

Design variables	Value
Input voltage [V]	380
Output power [W]	900
Rotational speed [r/min]	600
Poles/slots	8/12
Number of winding turns	185
Number of additional winding turns	1
Maximum residual flux density of PM [T]	0.42
Minimum air-gap length without eccentricity [μm]	800
Torque constant [N·m/A]	1.77
Outer diameter of rotor [mm]	108
Inner diameter of stator core [mm]	109.6
Outer diameter of motor [mm]	173

Fig. 2(a) shows a three-phase PM motor with eight poles and 12 slots which includes an additional winding. Table I shows the major specifications of the PM motor. The 2-D finite-element model developed in this study has an additional winding of one turn in teeth's 1, 2, and 3 in order to determine the fault detection signal induced in the additional winding by dynamic eccentricity, as shown in Fig. 2(a). The finite-element model consists of 127 800 triangle elements with three nodes, and 17 300 tetragonal elements with four nodes. The ferrite PM has a residual flux density of 0.42 T, and is magnetized in the radial direction. The air gap between the stator and the rotor is 800 μm, and the dynamic eccentricity is applied to the finite-element model from 0% to 50% with increments of 10%. We used the FLUX2D software to solve for the magnetic field by considering the nonlinear *B–H* characteristics of the stator core. The finite-element analysis was performed for each 1° rotation of the rotor during one revolution. The finite-element model was verified by comparing the simulated back EMF with the measured back EMF at the operating speed of 600 r/min. The simulated and measured back EMFs are 91.73 and 92.30 V, respectively, with an error of 0.62%.

Fig. 3 shows the simulated fault detection signal induced in the additional winding due to the dynamic eccentricity. In the case of no dynamic eccentricity, the fault detection signal induced in the additional winding is zero, as shown in Fig. 3(a). Fig. 3(b) shows the simulated fault detection signal induced in the additional winding for the PM motor for the case of 50% dynamic eccentricity. The dynamic eccentricity generates the fault detection signal induced in the additional winding. Fig. 3(c) shows the frequency spectrum of the fault detection signal induced in the additional winding for the PM motor for the case of 50% dynamic eccentricity. The sideband frequencies of the four-pole pair motor are the third- and fifth-frequency components, and the amplitudes of the third- and fifth-frequency components of the fault detection signal induced in the additional winding are 3.12 and 8.93 mV/krpm, respectively. Fig. 4 shows the peak-to-peak amplitude of the fault detection signal induced in the additional winding due to the amplitude of the dynamic eccentricity of the PM motor. The peak-to-peak amplitude of the

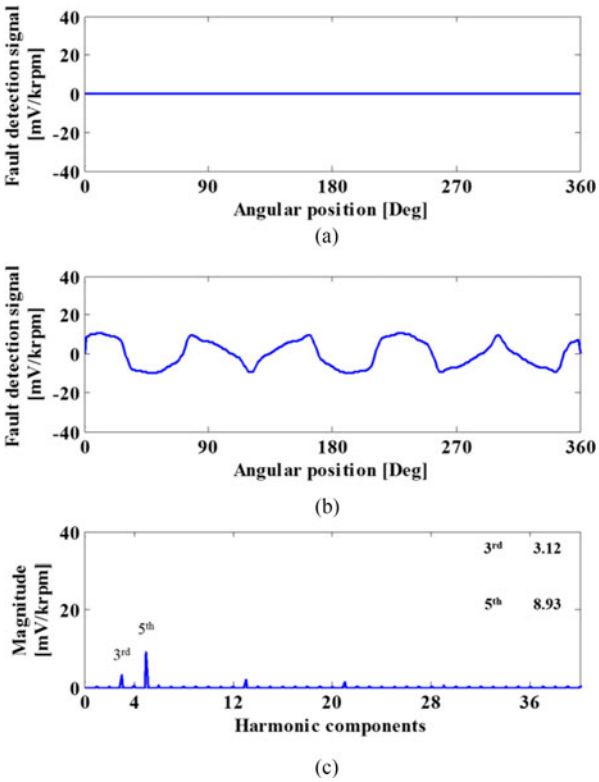

Fig. 3. Simulated (a) fault detection signal induced in the additional winding without eccentricity, for a PM motor with eight poles and 12 slots, (b) fault detection signal induced in the additional winding with 50% dynamic eccentricity, and (c) frequency spectrum of fault detection signal induced in the additional winding with 50% dynamic eccentricity.

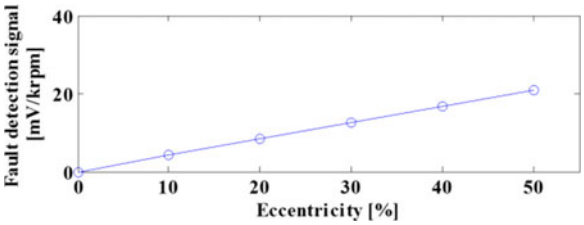

Fig. 4. Peak-to-peak amplitude of the fault detection signal induced in the additional winding due to the dynamic eccentricity of the PM motor with eight poles and 12 slots.

fault detection signal increases linearly with the increase of the dynamic eccentricity. Therefore, the dynamic eccentricity can be identified by monitoring the amplitude of the fault detection signal induced in the additional winding.

We also performed a finite-element analysis under nonstationary conditions in order to identify the fault detection signal with varying rotational speed. In this analysis, the rotational speed of the rotor increased linearly from 450 to 600 r/min over 2 s. A dynamic eccentricity of 50% is applied to the finite-element model. The finite-element analysis was performed during a 2-s period with 4000 steps. Fig. 5(a) shows the rotational speed of the rotor. Fig. 5(b) shows the simulated back EMF induced in the additional winding. The peak-to-peak amplitude of the back EMF induced in the additional winding increases as the rotational speed of rotor increases. Fig. 5(c) shows the simulated

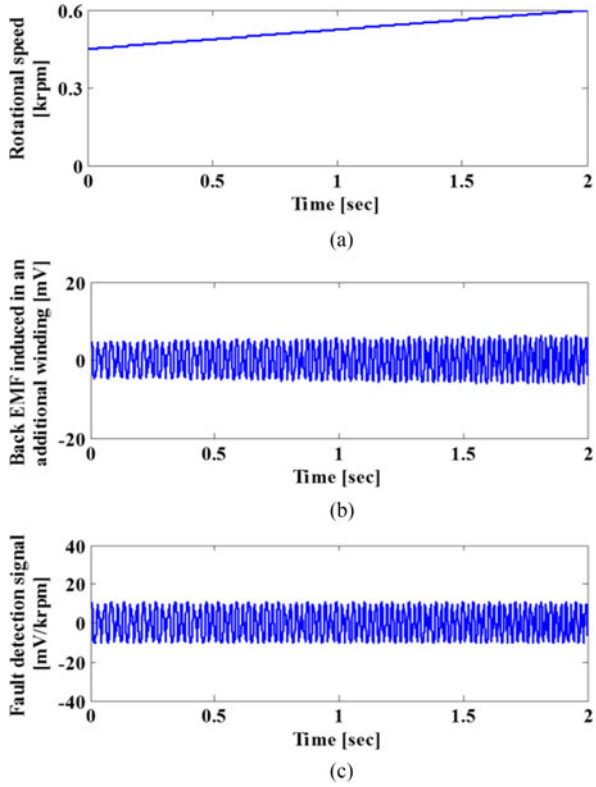

Fig. 5. (a) Rotational speed of the rotor, (b) simulated back EMF induced in the additional winding with 50% dynamic eccentricity, and (c) simulated fault detection signal induced in the additional winding with 50% dynamic eccentricity.

fault detection signal induced in the additional winding. The peak-to-peak amplitude of the fault detection signal induced in the additional winding is 20.85 V/kr/min which is constant, regardless of rotational speed. Therefore, the dynamic eccentricity can be detected by monitoring the fault detection signal induced in the additional winding, regardless of the rotational speed of the rotor.

IV. Experimental Details

In this study, we developed an experimental setup to measure the fault detection signal induced in the additional winding due to dynamic eccentricity, using a three-phase PM motor with eight poles and 12 slots, as shown in Fig. 6. In this experiment, the eccentric shaft housings that support the rotating shaft are prototyped to generate 25% and 50% dynamic eccentricity. Fig. 7(a) and (b) shows the concentric and 50% eccentric shaft housings, respectively. They are connected to the outer housing through two ball bearings, and the top and bottom of the shaft are inserted into the concentric or eccentric shaft housings, as shown in Fig. 6. The fault detection signal induced in the additional winding is measured at the operating speed of 600 r/min, and its operating speed is measured using an optical sensor (Keyence FU-10). The radial displacement of the rotating shaft is measured using a laser displacement sensor (Di-soric LAT 61 K 30/8), as shown in Fig. 6. Fig. 8 shows the additional winding which is composed of one turn of copper coil with a 1.4 mm

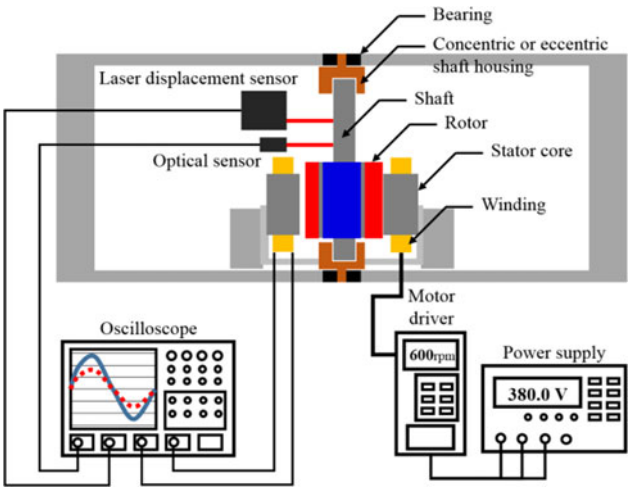

Fig. 6. Experimental setup to measure the dynamic eccentricity of the rotor and the back EMF induced in the additional winding of the PM motor with eight poles and 12 slots.

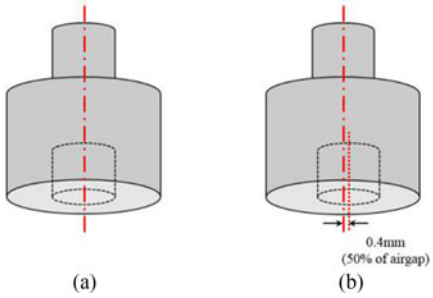

Fig. 7. (a) Concentric shaft housing and (b) 50% eccentric shaft housing.

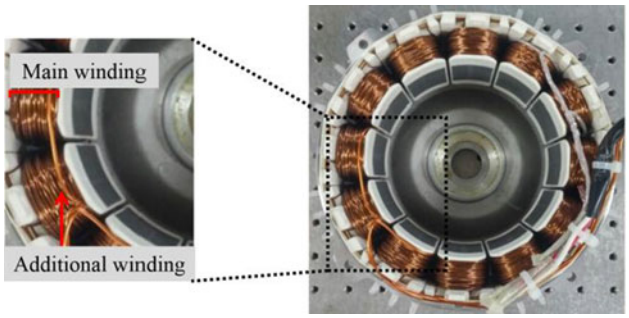

Fig. 8. Additional winding to measure the fault detection signal.

diameter, and they are wound around the outside of the main windings of teeth 1, 2, and 3. We measured the fault detection signal induced in the additional winding of the PM motor using an oscilloscope (LeCroy WaveRunner 6100A) and a voltage probe (LeCroy PP007-WR) with a measuring range of ± 300 V and a resolution of 0.001 mV.

Fig. 9(a) shows the measured radial displacement of the shaft of the rotor supported by the concentric shaft housing. The amplitude of radial displacement can be regarded as the amount of the dynamic eccentricity. Because of the manufacturing error of the concentric shaft housing and the unbalanced mass of the rotor, the radial displacement of the shaft is about 33.0 μm,

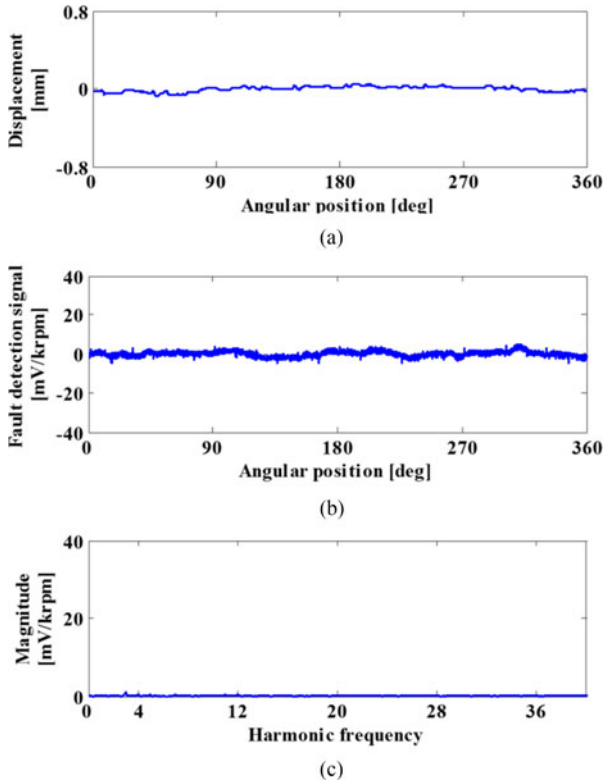

Fig. 9. Measured (a) radial displacement of the rotor supported by the concentric shaft winding, (b) fault detection signal induced in the additional winding without dynamic eccentricity, and (c) frequency spectrum of the fault detection signal induced in the additional winding without dynamic eccentricity.

which is 4.1% of the air-gap length. Fig. 9(b) shows the measured fault detection signal induced in the additional winding. The peak-to-peak amplitude of the fault detection signal induced in the additional winding is 9.76 mV/kr/min. Fig. 9(c) shows the frequency spectrum of the fault detection signal induced in the additional winding for the PM motor without eccentricity. Fig. 10(a) shows the measured radial displacement of the rotor supported by the eccentric shaft housing of 25% (200 μm). The radial displacement is about 203.2 μm, which is about 25.4% of the air-gap length. Fig. 10(b) shows the measured fault detection signal induced in the additional winding. The peak-to-peak amplitude of the fault detection signal induced in the additional winding is 15.81 mV/kr/min. Fig. 10(c) shows frequency spectrum of fault detection signal induced in the additional winding for the PM motor in the case of 25% dynamic eccentricity. The amplitudes of the third- and fifth-frequency components of the fault detection signal induced in the additional winding are 0.63 and 3.98 mV/krpm, respectively. Fig. 11(a) shows the measured radial displacement of the rotor supported by the eccentric shaft housing with 50% eccentricity (400 μm). The radial displacement is about 454.3 μm, which is about 56.8% of the air-gap length. Fig. 11(b) shows the measured fault detection signal induced in the additional winding. The peak-to-peak amplitude of the fault detection signal induced in the additional winding is 24.10 mV/kr/min. Fig. 11(c) shows the frequency spectrum of the fault detection signal induced in the additional winding

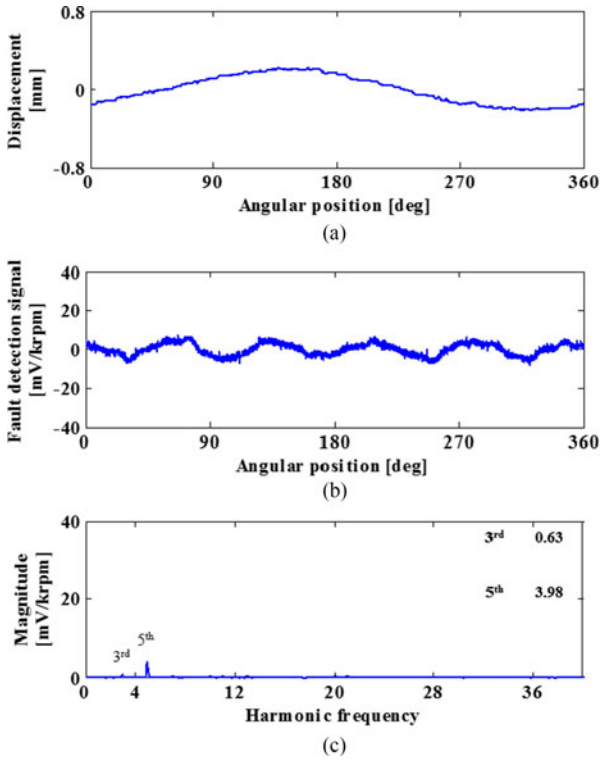

Fig. 10. Measured (a) radial displacement of the rotor supported by the eccentric shaft housing of 25% dynamic eccentricity, (b) fault detection signal induced in the additional winding with 25% dynamic eccentricity, and (c) frequency spectrum of the fault detection signal induced in the additional winding with 25% dynamic eccentricity.

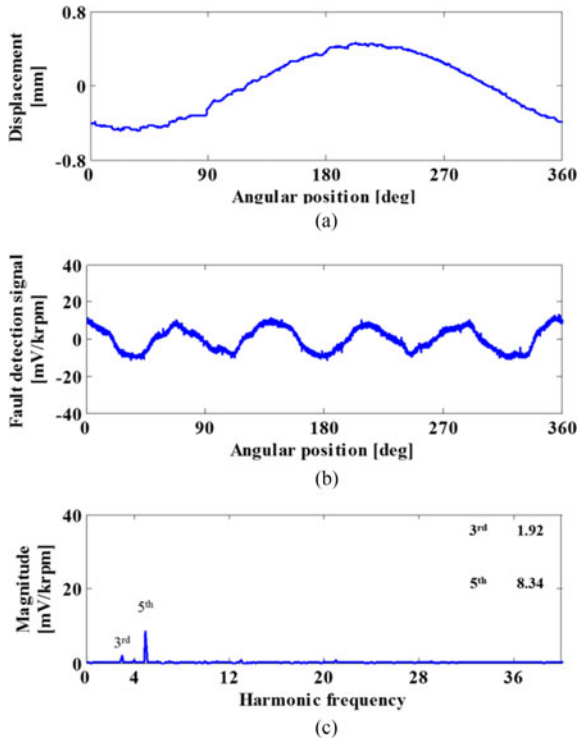

Fig. 11. Measured (a) radial displacement of the rotor supported by the eccentric shaft housing of 50% dynamic eccentricity, (b) fault detection signal induced in the additional winding with 50% dynamic eccentricity, and (c) frequency spectrum of the fault detection signal induced in the additional winding with 50% dynamic eccentricity.

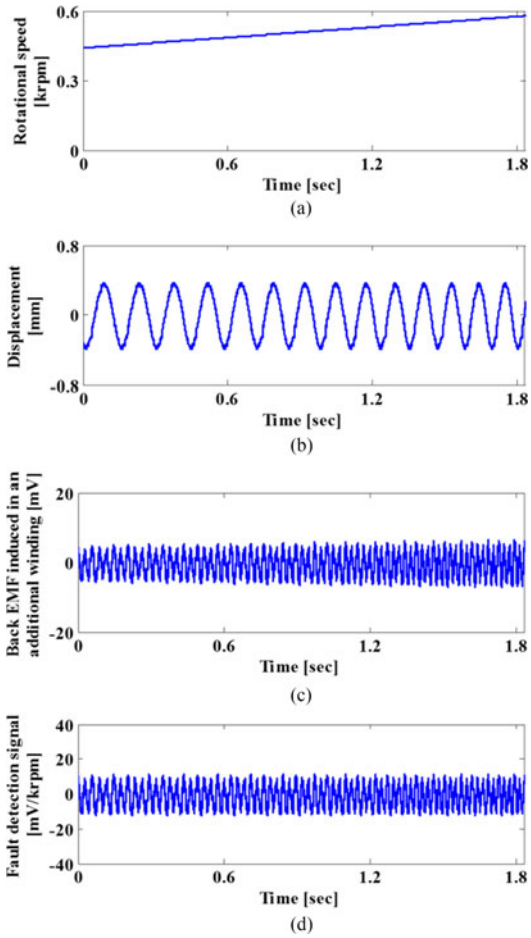

Fig. 12. Measured (a) rotational speed of the rotor, (b) radial displacement of the rotor supported by the eccentric shaft housing of 50% dynamic eccentricity, (c) back EMF induced in the additional winding with 50% dynamic eccentricity, and (d) fault detection signal induced in the additional winding with 50% dynamic eccentricity.

of the PM motor for the case of 50% dynamic eccentricity. The amplitudes of the third- and fifth-frequency components of the fault detection signal induced in the additional winding are 1.92 and 8.34 mV/krpm, respectively. This experiment shows that the dynamic eccentricity can be identified by monitoring the increase of the magnitude of the fault detection signal. Even though the proposed method does not need frequency analysis, the fault detection signal has the frequency components at the harmonics of $(kp \pm 1)$.

We also performed an experiment to measure the fault detection signal under nonstationary conditions. A dynamic eccentricity of 50% is applied in this experiment by using the eccentric shaft housing to support the rotating shaft. Fig. 12(a) shows the measured rotational speed of the rotor. The rotational speed increases linearly from 441 to 578 r/min over 1.832 s. Fig. 12(b) shows the measured radial displacement of the shaft of the rotor with the 50% eccentric shaft housing. Fig. 12(c) shows the back EMF induced in the additional winding. The peak-to-peak amplitude of the back EMF induced in the additional winding increases according to the rotational speed. Fig. 12(d) shows the measured fault detection signal

induced in the additional winding. The peak-to-peak amplitude of the fault detection signal induced in the additional winding is constantly 23.70 mV/kr/min. This experiment shows that the dynamic eccentricity can also be identified by monitoring the magnitude of the fault detection signal even under nonstationary conditions.

V. Conclusion

In this paper, we proposed a method to detect the dynamic eccentricity of a rotor in a PM motor by monitoring a fault detection signal induced in an additional winding in real time, without performing further postprocessing, even under nonstationary rotational speeds. We derived the mathematical equations of the fault detection signal which is the back EMF in an additional winding wound around the teeth corresponding to the even number of pole pitches divided by the angular speed. The proposed equations were verified by the finite-element analysis of a three-phase PM motor with eight poles and 12 slots. We also developed an experimental setup to measure the back EMF induced in an additional winding of a three-phase PM motor with eight poles and 12 slots with 25% and 50% dynamic eccentricities. We confirmed that the dynamic eccentricity generates the fault detection signal induced in the additional winding. The peak-to-peak amplitude of the fault detection signal induced in the additional winding increases linearly with dynamic eccentricity. Therefore, the dynamic eccentricity can be identified by monitoring the amplitude of the fault detection signal induced in the additional winding, regardless of rotational speed, without performing any further postprocessing. In real applications of a PM motor, there are static eccentricities as well as dynamic eccentricities. The proposed method in this paper cannot detect the static eccentricity of a rotor in a PM motor. However, for the mixed eccentricity in which both static and dynamic eccentricities exist, the proposed method can still detect the dynamic eccentricity of a rotor in a PM motor as the dynamic eccentric motion grows because the static eccentric motion does not change the corresponding air gap and the corresponding back EMF induced in the additional winding. The proposed method requires an additional winding. It may not be an easy task to install an additional winding to some of the existing motors in operation, but it is simple and economical method for newly manufactured motors. This research can be utilized to detect dynamic eccentric faults of PM motors, before failure events shut down the entire system, or cause serious damage.

References

[1] A. H. Bonnett and C. Yung, "Increased efficiency versus increased reliability," *IEEE Ind. Appl. Mag.*, vol. 14, no. 1, pp. 29–36, Jan./Feb. 2008.

[2] O. V. Thorsen and M. Dalva, "Methods of condition monitoring and fault diagnosis for induction motors," *Eur. Trans. Electr. Power*, vol. 8, no. 5, pp. 383–395, Sep. 1998.

[3] J. Rosero, J. Cusido, A. G. Espinosa, J. A. Ortega, and L. Romeral, "Broken bearings fault detection for a permanent magnet synchronous motor under non-constant working conditions by means of a joint time frequency analysis," in *Proc. IEEE Int. Symp. Ind. Electron.*, 2007, pp. 3415–3419.

[4] J. Rosero, J. L. Romeral, J. Cusido, J. A. Ortega, and A. Garcia, "Fault detection of eccentricity and bearing damage in a PMSM by means of wavelet transforms decomposition of the stator current," in *Proc. 23rd Annu. IEEE Appl. Power Electron. Conf. Expo.*, 2008, pp. 111–116.

[5] M. Pacas, S. Villwock, and R. Dietrich, "Bearing damage detection in permanent magnet synchronous machines," in *Proc. IEEE Energy Convers. Congr. Expo.*, 2009, pp. 1098–1103.

[6] C. P. Mbo'o, T. Herold, and K. Hameyer, "Impact of the load in the detection of bearing faults by using the stator current in PMSM's," in *Proc. Int. Conf. Elect. Mach.*, 2014, pp. 1621–1627.

[7] C. P. Mbo'o and K. Hameyer, "Modeling of a permanent-magnet excited synchronous machine with bearing damage," in *Proc. 40th Annu. Conf. IEEE Ind. Electron. Soc.*, 2014, pp. 3855–3860.

[8] S. M. Mirimani, A. Vahedi, F. Marignetti, and E. D. Santis, "Static eccentricity fault detection in single-stator–single-rotor axial-flux permanent-magnet machines," *IEEE Trans. Ind. Appl.*, vol. 48, no. 6, pp. 1838–1845, Nov./Dec. 2012.

[9] W. Le Roux, R. G. Harley, and T. G. Habetler, "Detecting rotor faults in low power permanent magnet synchronous machines," *IEEE Trans. Power Electron.*, vol. 22, no. 1, pp. 322–328, Jan. 2007.

[10] J. Rosero, J. Cusido, J. A. Ortega, A. Garcia, and L. Romeral, "On-line condition monitoring technique for PMSM operated with eccentricity," in *Proc. IEEE Int. Symp. Diagn. Electr. Mach., Power Electron. Drives*, 2007, pp. 95–100.

[11] J. Rosero, L. Romeral, E. Rosero, and J. Urresty, "Fault detection in dynamic conditions by means of discrete wavelet decomposition for PMSM running under bearing damage," in *Proc. 24th Annu. IEEE Appl. Power Electron. Conf. Expo.*, 2009, pp. 951–956.

[12] S. Rajagopalan, W. L. Roux, T. G. Habetler, and R. G. Harley, "Dynamic eccentricity and demagnetized rotor magnet detection in trapezoidal flux (brushless DC) motors operating under different load conditions," *IEEE Trans. Power Electron.*, vol. 22, no. 5, pp. 2061–2069, Sep. 2007.

[13] B. M. Ebrahimi, J. Faiz, and M. J. Roshtkhari, "Static-, dynamic-, and mixed-eccentricity fault diagnoses in permanent-magnet synchronous motors," *IEEE Trans. Ind. Electron.*, vol. 56, no. 11, pp. 4727–4739, Nov. 2009.

[14] B. M. Ebrahimi and J. Faiz, "Diagnosis and performance analysis of three phase permanent magnet synchronous motors with static, dynamic and mixed eccentricity," *IET Elect. Power Appl.*, vol. 4, no. 1, pp. 53–66, Jan. 2010.

[15] B. M. Ebrahimi, J. Faiz, and B. N. Araabi, "Pattern identification for eccentricity fault diagnosis in permanent magnet synchronous motors using stator current monitoring," *IET Elect. Power Appl.*, vol. 4, no. 6, pp. 418–430, Jul. 2010.

[16] B. M. Ebrahimi, M. J. Roshtkhari, J. Faiz, and S. V. Khatami, "Advanced eccentricity fault recognition in permanent magnet synchronous motors using stator current signature analysis," *IEEE Trans. Ind. Electron.*, vol. 61, no. 4, pp. 2041–2052, Apr. 2014.

[17] C. Bruzzese, "Diagnosis of eccentric rotor in synchronous machines by analysis of split-phase currents; Part II: Experimental analysis," *IEEE Trans. Ind. Electron.*, vol. 61, no. 8, pp. 4206–4216, Aug. 2014.

[18] J. Hong, S. B. Lee, C. Kral, and A. Haumer, "Detection of airgap eccentricity for permanent magnet synchronous motors based on the d-axis inductance," in *Proc. IEEE Int. Symp. Diagn. Elect. Mach., Power Electron. Drives*, 2011, pp. 378–384.

[19] J. Hong, D. Hyun, T. J. Kang, S. B. Lee, C. Kral, and A. Haumer, "Detection and classification of rotor demagnetization and eccentricity faults for PM synchronous motors," in *Proc. IEEE Energy Convers. Congr. Expo.*, 2011, pp. 2512–2519.

[20] D. Torregrossa, A. Khoobroo, and B. Fahimi, "Prediction of acoustic noise and torque pulsation in PM synchronous machines with static eccentricity and partial demagnetization using field reconstruction method," *IEEE Trans. Ind. Electron.*, vol. 59, no. 2, pp. 934–944, Feb. 2012.

[21] B. M. Ebrahimi and J. Faiz, "Magnetic field and vibration monitoring in permanent magnet synchronous motors under eccentricity fault," *IET Elect. Power Appl.*, vol. 6, no. 1, pp. 35–45, Jan. 2012.

[22] A. Rezig, M. R. Mekideche, and A. Djerdir, "Effect of rotor eccentricity faults on noise generation in permanent magnet synchronous motors," *Prog. Electromagn. Res. C*, vol. 15, pp. 117–132, 2010.

[23] A. Rezig, M. R. Mekideche, and A. Djerdir, "Impact of eccentricity and demagnetization faults on magnetic noise generation in brushless permanent magnet DC motors," *J. Elect. Eng. Technol.*, vol. 6, no. 3, pp. 356–363, May 2011.

[24] J. F. Gieras, C. Wang, and J. C. Lai, *Noise of Polyphase Electric Motors*. Boca Raton, FL, USA: CRC Press, 2006.

[25] Z. Q. Zhu and D. Howe, "Instantaneous magnetic field distribution in brushless permanent magnet DC motors. III. Effect of stator slotting," *IEEE Trans. Magn.*, vol. 29, no. 1, pp. 143–151, Jan. 1993.

[26] R. Perers, U. Lundin, and M. Leijon, "Saturation effects on unbalanced magnetic pull in a hydroelectric generator with an eccentric rotor," *IEEE Trans. Magn.*, vol. 43, no. 10, pp. 3884–3890, Oct. 2007.

Kyungjin Kang received the B.S. degree in mechanical engineering and the Ph.D. degree in mechanical convergence engineering from Hanyang University, Seoul, South Korea, in 2010 and 2017, respectively.

He is currently a Researcher with HYUNDAI MOBIS. His current research focuses on the development and analyses of synchronous electric motors for electrical vehicle propulsion.

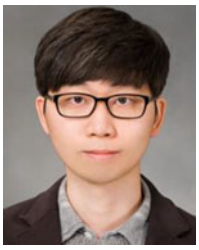

Jeongyong Song received the B.S. degree in mechanical engineering from Hanyang University, Seoul, South Korea, in 2012, where he is currently working toward the Ph.D. degree in mechanical convergence engineering.

His current research focuses on the development of electric motors and reduction of magnetically induced vibration and noise of electric motors for consumer electronics.

Chiho Kang received the B.S. degree in mechanical engineering and the M.S. degree in mechanical convergence engineering from Hanyang University, Seoul, South Korea, in 2011 and 2015, respectively, where he is currently working toward the Ph.D. degree in mechanical convergence engineering.

His current research focuses on the coupled analyses of electric motors for electric vehicles due to magnetic and structural interactions.

Sangjin Sung received the B.S. and M.S. degrees in mechanical engineering and the Ph.D. degree in mechanical convergence engineering from Hanyang University, Seoul, South Korea, in 2008, 2010, and 2015, respectively.

He is currently a Researcher with LG Electronics. His current research focuses on the noise and vibration analyses due to electromagnetic excitation in electric motors for consumer electronics.

Gunhee Jang (M'00) received the B.S. degree from Hanyang University, Seoul, South Korea, in 1984, the M.S. degree from Korea Advanced Institute of Science and Technology, Seoul, in 1986, and the Ph.D. degree from the University of California, Berkeley, CA, USA, in 1993, all in mechanical engineering.

He is currently a Professor in the Department of Mechanical Engineering and the Director of the Precision Rotating Electromechanical Machine Laboratory, Hanyang University. He has authored or coauthored more than 300 articles published in journals and conference proceedings in his field and more than 30 patents including several international patents. His current research focuses on the analysis, design, and control of electromechanical systems, such as motors and actuators and microrobots actuated by magnetic navigation systems.